Precipitation behavior of Cu-3.0Ni-0.72Si alloy

Jiang Yi [a], Yanlin Jia [a, b, *], Yuyuan Zhao[c], Zhu Xiao [a, d*], Kejian He [a], Qi Wang [a], Mingpu Wang [a], Zhou Li[a, e, *]

[a] School of Materials Science and Engineering, Central South University, Changsha, 410083, China

[b] College of Materials Science and Engineering, Beijing University of Technology, Beijing, 100124, China

[c] School of Engineering, University of Liverpool, Liverpool L69 3GH, UK

[d] Key Laboratory of Nonferrous Metal Materials Science and Engineering, Ministry of Education, Changsha, 410083, China

[e] State Key Laboratory of Powder Metallurgy, Changsha, 410083, China

* Corresponding authors

E-mail addresses: jiayanlin@126.com (Yanlin Jia), xiaozhumse@163.com (Zhu Xiao), lizhou6931@csu.edu.cn (Zhou Li)

Abstract: Cu-Ni-Si alloys have been widely applied in electronic and electrical industries. The precipitation behavior of some of the Cu-Ni-Si alloys is still not well understood. In this study, the precipitation behavior of the Cu-3.0Ni-0.72Si alloy aged at 600℃ for different times was investigated by transmission electron microscopy, atom probe tomography and phenomenological theory of precipitation crystallography. A new orientation relationship (OR) between the precipitates and the Cu matrix was found in the over-aged condition and a coarsening mechanism of the metastable precipitates was put forward. The two- and three-dimension invariant line theories were successfully applied in interpreting the evolution of the ORs and the morphologies in the Cu/δ system. At the early stage of aging, the fine metastable $(Cu,Ni)_2Si$ precipitates are coherent with the Cu matrix, with a quasi-Bain OR of $(110)_{Cu}||(100)_{\delta}$ and $[001]_{Cu}||[001]_{\delta}$, and four pairs of parallel conjugate planes: $(\bar{1}\bar{1}1)_{Cu}||(\bar{3}01)_{\delta}$, $(111)_{Cu}||(301)_{\delta}$, $(\bar{1}11)_{Cu}||(021)_{\delta}$, and $(1\bar{1}1)_{Cu}||(0\bar{2}1)_{\delta}$. The precipitates have a δNi_2Si structure, with some Ni atoms substituted by Cu atoms. During growth, the core region of the metastable $(Cu,Ni)_2Si$ precipitate transforms into stable δNi_2Si, with a quasi-NW OR of $(\bar{1}11)_{Cu}||(021)_{\delta}$ and $[110]_{Cu}||[100]_{\delta}$, while a layer of metastable $(Cu,Ni)_2Si$ still exists around the core. With prolonging aging time, the δNi_2Si precipitates with the OR of $(\bar{1}11)_{Cu}||(021)_{\delta}$ and $[110]_{Cu}||[100]_{\delta}$ grow two-dimensionally to form a plate-like shape, while those with the OR of $(111)_{Cu}||(301)_{\delta}$ and $[\bar{1}10]_{Cu}||[010]_{\delta}$ grow one-dimensionally to form a fiber-like shape.

1. Introduction

Cu-Ni-Si alloys have been widely used in electronic and electrical industries, e.g., semiconductor lead-frames, electrical contacts and connector components, due to the combination of high strength and high electrical conductivity [1-6]. The combined high strength and high conductivity of Cu-Ni-Si alloys are attributed to the precipitation of nanoscale particles during aging. Understanding and optimization of the aging process to control the precipitation process are therefore the key to improve the overall property of any Cu-Ni-Si alloy.

A large amount of research has been carried out in the last few decades to investigate the precipitation behavior of Cu-Ni-Si alloys. It is well accepted that the main stable precipitate is the δNi_2Si intermetallic compound (δ) [4, 6-10], especially in the Cu-Ni-Si alloys with Ni content less than 5 wt.%, although βNi_3Si [11], γNi_5Si_2 [12], $(Cu, Ni)_3Si$ [7], $Cu_3Ni_5Si_2$ [13] and Ni_3Si_2 [13] also exist in the alloys. The δ phase was first identified in a quasi-binary section of the ternary Cu-Ni-Si phase diagram [14] and the crystal structure of pure δNi_2Si was determined as the orthorhombic system with a *Pbnm* space group (a_δ=7.06Å, b_δ=4.99Å, c_δ=3.72Å) [15]. Teplitskiy *et al.* [16] suggested that the δ precipitates in Cu-Ni-Si alloys with low Ni and Si contents had a disk-like shape, lying on $\{1\ 1\ 0\}_{Cu}$, which was confirmed by Cho *et al.* [17] and Jia *et al.* [18] in the Cu-1.5Ni-xSi (in wt%) alloys. The sequence of formation of the δ precipitates in the Cu-2.4Ni-0.7Si-0.4Cr (wt%) alloy at 450℃ was summarized by Hu *et al.* [4] as follows: supersaturated solid solution $\rightarrow \delta_1Ni_2Si \rightarrow \delta_1Ni_2Si$ (rotated) $\rightarrow \delta_2Ni_2Si$, while Lee *et al.*

[13] suggested that the precipitation sequence in a torsion-deformed Cu-2.9Ni-0.6Si alloy was: $Cu_3Ni_5Si_2 \rightarrow Ni_3Si_2 \rightarrow$ stable Ni_2Si. The orientation relationship (OR) between the matrix and the δ phase was first reported as $[0\ 0\ 1]_{Cu}||[0\ 0\ 1]_{\delta}$ and $(1\ 1\ 0)_{Cu}||(1\ 0\ 0)_{\delta}$ [19, 20]. Hu *et al.* [4] reported that the first precipitate formed (δ_1Ni_2Si) had this OR, but it rotated slightly during aging and subsequently transformed into the δ_2Ni_2Si precipitate, which had the OR of $[1\ 1\ 0]_{Cu}||[0\ 1\ 0]_{\delta}$ and $(1\ \bar{1}\ 1)_{Cu}||(3\ 0\ 1)_{\delta}$. An additional OR of $(1\ 1\ 0)_{Cu}||(2\ 1\ \bar{1})_{\delta}$ and $[1\ 1\ \bar{2}]_{Cu}||[3\ 2\ 4]_{\delta}$ has also been found in the Cu-8.0Ni-1.8Si-0.15Mg alloy [21]. Formation of a fiber-shaped δNi_2Si phase (discontinuous precipitates) in the over-aging stage, with the OR of $[1\ 1\ 0]_{Cu}||[0\ 1\ 0]_{\delta}$ and $(1\ \bar{1}\ 1)_{Cu}||(3\ 0\ 1)_{\delta}$, was recently reported [5, 22-24].

Whilst the research to date has provided valuable information on the precipitation behavior in Cu-Ni-Si alloys, there are still a number of issues to be resolved. First, there exist different views on the composition, structure and coarsening mechanism of the primary precipitates. Early work considered that the primary phases are formed from a modulated structure of Si-rich and Si-poor regions due to the spinodal decomposition and the precipitate is an ordered $(Cu, Ni)_3Si$ with the DO_{22} structure [7]. Recent transmission electron microscopy (TEM) studies have shown that the primary precipitate had a δNi_2Si structure, about 3-4 nm in diameter [4, 18]; however, no information on the atomic level elemental distribution was available to confirm the result. Lee *et al.* [13] observed $Cu_3Ni_5Si_2$ particles (~4 nm) by atom probe tomography (APT), but no structure information was given. The roles of Si, Ni and Cu in the growth process of the precipitates

are still not clear. Second, the majority of the work on the morphology of the δ particles considered the broad interface, without much consideration of the details of the edge facets, and observed edge-on habit interfaces [4, 18]. In fact, the edge facets are locations where stress concentration is more likely to occur under loading. The morphological evolution of the precipitates is important for understanding the age hardening effect. In addition, the details of the interface, including the shape of and the defects on the major planes of the δ particles, can also affect the stress state and accordingly the strength of the alloy, but they have hardly been studied. Third, the nature of the ORs between the precipitates and the matrix is not fully understood yet. Although several ORs have been observed in Cu-Ni-Si alloys, new ORs may exist. Furthermore, the ORs are closely related to the nucleation, growth and morphological evolution of the precipitates and therefore have a strong influence on the strength [25]. Mechanistic understanding of the relationship between the OR and the morphology of the precipitates is important.

In this study, the precipitation behavior of the Cu-3.0Ni-0.72Si (wt.%) alloy was investigated by employing spherical aberration corrected transmission electron microscopy (ACTEM), high resolution transmission electron microscopy (HRTEM), atom probe tomography (APT) and the phenomenological theory of precipitation crystallography. The microstructures, morphologies, compositions and ORs of the precipitates at the initial and late aging stages were examined in detail. The evolution of the ORs was analyzed and a new OR was found at the late stage of aging. The elemental distribution in the precipitates at different aging stages was analyzed by APT at the atomic

level, enabling the proposition of a new metastable transition and coarsening mechanism of precipitates. The evolutions of the ORs and the morphologies of the precipitates were interpreted by the two-dimensional invariant line (2DIL) and the three-dimensional invariant line (3DIL) theories.

2. **Materials and Experimental Methods**

2.1 Preparation of specimens

The Cu-3.0Ni-0.72Si alloy was melted in a medium-frequency induction furnace and a 35mm-thick ingot was cast in an iron mold under a N_2 atmosphere. After homogenization at 960℃ for 4 h, the ingot was hot rolled at 850℃ into a plate by an 85% reduction. The test specimens were cut from the hot rolled plate, solution-treated at 980℃ for 4h, followed by water quenching and then aging at 600℃ for different times.

2.2 Microstructural characterization

The specimens for TEM observations had a diameter of 3 mm and were first ground mechanically to a thickness of around 80 μm and then electro-polished by a Struers Tenpol-5 twin-jet unit, using a mixed solution of nitric acid and methyl alcohol, with a voltage of 10 V and a temperature of around -35°C. A Gatan 691 dual-mill precision ion polishing system (PIPS) was also used wherever necessary. The TEM and HRTEM observations were conducted on a Tecnai G2 F20 and Titan G2 60-300, respectively.

The specimens for APT observations had dimensions of $0.5\times0.5\times20$ mm^3 and were

prepared by the standard two-step electro-polishing procedure. APT observations were performed on a LEAP 4000 HR, under a temperature of 50 K, a pulse repetition rate of 200 kHz and a pulse voltage fraction of 15%. The standing voltage on the needle specimen was varied automatically in order to maintain an evaporation rate of 5 ions every 1000 pulses. The background vacuum level of the analysis chamber was kept at less than10^{-8} Pa. The detection efficiency of the instrument was 36%. The reconstruction and quantitative analysis of the APT data were carried out using the IVAS 3.6.12 software.

3. Results and discussion

3.1 Evolution of microstructure and OR during aging

Fig. 1a shows the variation of the hardness of the Cu-3.0Ni-0.72Si alloy aged at 600℃, with approximate boundaries between different aging stages indicated. The hardness increased significantly with aging time up to 4 minutes (under-aging stage) and reached a plateau from 4 to 30 minutes (peak-aging stage). The hardness decreased gradually with increasing aging time further (over-aging stage). It is well accepted that the increase in hardness in the under-aging stage can be attributed to the formation of primary precipitates and the decrease in the over-aging stage to the growth of the precipitates. To investigate the evolution of the precipitates, the specimens aged for 30 seconds and 8 hours were chosen as representative conditions for clearly under-aging and over-aging stages, respectively.

Figs. 1b and 1c show the bright-field TEM images of the Cu-3.0Ni-0.72Si alloy aged at

600℃ for 30 s and 8 hrs, respectively, viewed along the zone axis of $[001]_{Cu}$. Ultrafine precipitates, with an average size of about 5 nm, were distributed uniformly and densely in the specimen aged for 30 s (Fig.1b). These precipitates coarsened dramatically to larger sizes of 50-100nm after 8 hrs aging, with a much lower density of distribution (Fig.1c). For convenience, the precipitates in the specimens aged for 30 s and 8 h are designated as nascent precipitates (NPs) and ripe precipitates (RPs), respectively.

The morphology and crystallographic characteristics of the NPs are shown in Fig. 2. Figs. 2a, 2c and 2e show the typical HRTEM images viewed along $[\bar{1}10]_{Cu}$, $[110]_{Cu}$ and $[1\bar{1}2]_{Cu}$, respectively. The Fast Fourier Transform (FFT) patterns corresponding to the HRTEM images in Figs. 2a, 2c and 2e are shown in Figs. 2b, 2d, 2f and 2g. Fig. 2h illustrates the morphology of a NP and its OR with the Cu matrix, which is labelled as OR_{NP} in this paper for simplification.

The NPs have a disk-like shape, with a large diameter-thickness ratio (~5 nm in diameter and ~2 nm in thickness). The disc planes of the NPs lie on the $\{110\}_{Cu}$ planes with a high coherency (Figs. 2a, 2c and 2e) and no sharp precipitate/matrix interfaces exist around the edges of the disc planes (Fig. 2c). There are lobe-shaped strain fields distributed around the disc planes (Figs. 2a and 2e). However, no interfacial defects, including dislocations and structure ledges, could be observed, because of the high coherency between the two phases (Fig. 2c).

The FFT results show that the NPs possess a δNi_2Si crystal structure, as evidenced by the superlattice spots of the δNi2Si phase. The ORs between the NPs and the Cu matrix can be expressed as $[110]_{Cu}||[100]_{\delta}$, $[\bar{1}10]_{Cu}||[010]_{\delta}$, and $[002]_{Cu}||[002]_{\delta}$, consistent with the results in Ref [4, 18]. There is a significant structure detail, which has not been reported in the literature to date, that the spots of four pairs of conjugate planes ($\{3\,0\,1\}_{\delta}/\{1\,1\,1\}_{Cu}$, $\{0\,2\,1\}_{\delta}/\{1\,1\,1\}_{Cu}$) are coincident (pink circles in Figs. 2b and 2d). It indicates that the corresponding conjugate planes are parallel in this under-aging stage, due to the high coherency between the NPs and the Cu matrix. Figs. 2f and 2g, with the zone axes of exactly $[1\ \bar{1}\ 2]_{Cu}||[0\ \bar{1}\ 2]_{\delta}$, also confirm that the corresponding conjugate planes, $(\bar{1}\ 1\ 1)_{Cu}/(0\ 2\ 1)_{\delta}$, are parallel. To sum up, the OR between the NPs and the Cu matrix is $(110)_{Cu}||(100)_{\delta}$ and $[001]_{Cu}||[001]_{\delta}$, with four pairs of parallel conjugate planes: $(\bar{3}01)_{\delta}||(\bar{1}\bar{1}1)_{Cu}$, $(301)_{\delta}||(111)_{Cu}$, $(021)_{\delta}||(\bar{1}11)_{Cu}$ and $(0\bar{2}1)_{\delta}||(1\bar{1}1)_{Cu}$.

The morphology and crystallographic characteristics of the RPs are shown in Fig. 3. Figs. 3a, 3c and 3e show the typical HRTEM images viewed along $[\bar{1}10]_{Cu}$, $[110]_{Cu}$ and $[1\bar{1}\,2]_{Cu}$, respectively. Figs. 3f, 3g and 3h show enlarged HRTEM images of selected areas in Fig. 3e. Figs. 3b and 3d are the FFT patterns corresponding to Figs. 3a and 3c, respectively, while Fig. 3i shows an inversed FFT image of Fig. 3h. Fig. 3j illustrates the morphology of a RP and its OR with the Cu matrix, which is labeled as OR_{RP} in this paper.

Similar to the NP, the RP also has a structure of δNi_2Si. The morphology of the RPs, however, is considerably different from that of the NPs. After 8 h aging, the RPs became

large, about 100 nm in length. The RPs have a plate-like shape, with a large diameter-thickness ratio (60~100 nm in diameter and 5~10 nm in thickness), suggesting a much larger growth rate along the radial direction than the thickness direction. The habit plane of the RPs is still the $(1\ 0\ 0)_{\delta}$ plane (F1), but its edge is made up of several parallel facets (Fig. 3c) rather than an indistinctive edge-on interface as in the case of the NPs. Two groups of characteristic facets, $(021)_{\delta}$ and $(0\bar{2}1)_{\delta}$, have been found among more than 10 RPs examined in this work. In the HRTEM image taken along the $[1\bar{1}2]_{Cu}$ zone axis (Fig. 3e), both the $(100)_{\delta}$ plane (F1) and the $(021)_{\delta}$ plane (F2) are edge-on, while the other planes (F3) are stepped facets composed of F1 and F2 (Fig. 3g). This observation helps to explain the oval or round shape of the habit planes reported in the previous works [4, 16, 19]. In addition, many interface defects, such as periodic interface dislocations (Fig. 3i), appeared around the RP, with a reduced range of strain fields. These interfacial structural ledges and dislocations can relieve interfacial stress and reduce the interface energy.

The OR of the RPs is quite different from the NPs. Fig. 3b shows two separate pairs of conjugate spots ($\{111\}_{Cu}/\{301\}_{\delta}$), indicating that the $\{301\}_{\delta}$ planes are no longer parallel to the conjugate $\{111\}_{Cu}$ planes and have an angle of about 2.52°. For the other two pairs of conjugate planes ($\{111\}_{Cu}/\{021\}_{\delta}$) observed along the $[110]_{Cu}\|[100]_{\delta}$ direction (Fig. 3d), the have a 2.46° deviation instead of remaining parallel to each other, although the $(\bar{1}11)_{Cu}$ plane is still parallel to the $(021)_{\delta}$ plane. A deviation angle of 1.23°, which is half of the angle between the $(1\bar{1}1)_{Cu}$ plane and the $(0\bar{2}1)_{\delta}$ plane, also exists between the

$(002)_{Cu}$ plane and the $(002)_{\delta}$ plane. Fig. 3e, with the axis zone of $[1\bar{1}2]_{Cu}$, also shows that the $[0\bar{1}2]_{\delta}$ is equivalent to the beam direction, indicating $[1\bar{1}2]_{Cu}||[0\bar{1}2]_{\delta}$ exactly.

The results above show that the RPs have a crystallographic rotation (R_{σ}) of 1.23° around the $[110]_{Cu}||[100]_{\delta}$ direction, which is different from the NPs. The OR between the RPs and the matrix can be expressed as: $(\bar{1}11)_{Cu}||(021)_{\delta}$, $[110]_{Cu}||[100]_{\delta}$, with $(\bar{1}\bar{1}1)_{Cu}$ $\Gamma(301)_{\delta}$, $(111)_{Cu}\Gamma(301)_{\delta}$, and $(1\bar{1}1)_{Cu}\Gamma(0\bar{2}1)_{\delta}$. The precipitates are still lying on the $(110)_{Cu}$ plane, but a slight crystallographic rotation around the normal direction of the habit plane has occurred during the transition from under-aging to over-aging.

The HRTEM images and the corresponding FFT patterns in Figs. 2 and 3 showed that the crystal structure of the precipitates formed in the Cu matrix at the initial stage of aging is δNi_2Si and changes little during aging. The lengths of the principal axes of the Cu/δ system, however, have changed from the under-aging state to the over-aging state (Table 1). The differences in lattice parameter between the precipitates and the Cu matrix increase as the δ precipitates grow larger. The lattice parameters of the RPs are closer to the lattice parameters of a pure, strain-free powder obtained by Toman [15], compared to those of the NPs.

3.2 Compositional change and growth mechanism

Fig. 4 shows the tomographies and compositions of the NP and RP in the Cu-3.0Ni-0.72Si alloy on an atomic level obtained by APT, revealing elemental distributions of Cu, Ni and

Si. Fig. 4a shows the tomographies of NPs, with the boundaries delineated as isoconcentration surfaces containing 40 at% (Ni, Si). Fig. 4b shows the compositional profiles plotted through one cross section of a single NP, while the inset shows elemental distributions of Cu, Ni and Si in the analyzed volume as indicated in Fig. 4a. Fig. 4c shows the tomography of a RP, highlighted by double-layer isoconcentration surfaces. The inner surface (smooth surface) encompasses the region containing 95 at% or more (Ni, Si), while the outer surface (mesh surface) encloses the region containing 33 at% or more (Ni, Si). Fig. 4d shows the compositional profiles of Cu, Ni and Si through one cross section of the RP.

The NP apparently contains Cu atoms across the whole NP and the Cu concentration decreases rapidly from the surface towards the core region of the NP. In the core region of the NP, the Si concentration does not change much, while the concentrations of Cu and Ni are approximately complementary to each other. As the atomic ratio of (Cu,Ni) to Si is close to 2, the NP can be identified as a metastable $(Cu, Ni)_2Si$ phase.

The RP has two distinctive regions separated by the inner isoconcentration surface (Fig. 4c), as indicated by the two inner vertical dashed lines (Fig. 4d). The core region (I) contains Ni and Si with a Ni/Si ratio of 2:1, showing a stable δNi_2Si phase. The outer region (II) is a 2-nm-thick layer around the core where Si approaches saturation and the concentrations of Cu and Ni are complementary to each other, indicating a metastable $(Cu, Ni)_2Si$ phase at the interface between the RP and the Cu matrix.

According to the APT results above, a reasonable growth mechanism of the precipitates, i.e. the coarsening from a NP to a RP as illustrated in Fig. 5, can be put forward. At the initial stage of aging, the metastable phase $(Cu,Ni)_2Si$ with a δNi_2Si crystal structure, namely the NP, is formed on the $\{1\ 1\ 0\}_{Cu}$ planes. The lattice parameters of the NP are dependent on the Cu content of the NP. A high Cu content leads to lattice parameters closer to those of the Cu matrix. The lattice mismatch between the NP and the Cu matrix is reconciled by the coherent strain fields near the interface. Due to the coordination of the composition and strain field at the interface, the metastable phase $(Cu,Ni)_2Si$ has a high coherency with the Cu matrix, resulting in a parallel relationship among the four pairs of conjugate planes. With prolonging aging time, the metastable phase grows as the Si content reaches the saturation concentration and the Cu atoms in the metastable phase are continuously being substituted by external Ni atoms. When the precipitate reaches a critical size, the core of the metastable phase turns into a stable δNi_2Si precipitate. This δNi_2Si core has a relatively large difference in lattice parameter with the Cu matrix, resulting in an interface stress. When the accumulation of the interface stress reaches a critical stage, it is released by the formation of interface defects, leading to a slight crystallographic rotation and the reduction of strain fields.

3.3 Interpretation of OR evolution by 2DIL theory

The high coherency in the Cu/δ system at the initial stage of aging results in the parallel relations of four pairs of conjugate planes. For a diffusion transformation, however, the

lattice parameters change constantly during aging due to changing elemental and stress conditions. Nonetheless, one pair of conjugate planes, $(\bar{1}11)_{Cu}/(021)_{\delta}$, keeps the parallel relationship. The 2DIL theory, which has been proved to be an efficient approach to predict the OR transformation between two phases [25, 26], is applied here to interpret the OR evolution between the precipitates and the Cu matrix.

In the 2DIL theory, the OR transformation is determined by lattice distortion and a rigid rotation on a certain plane to reduce interface energy by forming an invariant line, although the real process is actually affected by many factors such as composition, stress state and interface defects. The transformation from OR_{NP} to OR_{RP} can be described by a rotation around the normal direction of the habit plane and can be treated as a 2DIL problem on the habit plane. The rotation angle, θ, to satisfy the 2DIL condition can be calculated by [25]:

$$\cos\theta = (1 + ab)/(a + b) \quad (1)$$

where $a = \frac{[001]_{\delta}}{[001]_{Cu}} = \frac{c_{\delta}}{a_{Cu}}$ (>1) is an expansion along the $[001]_{Cu}$ direction and $b = \frac{[010]_{\delta}}{[\bar{1}10]_{Cu}} = \frac{b_{\delta}}{\sqrt{2}a_{Cu}}$ (<1) is a contraction along the $[\bar{1}\ 1\ 0]_{Cu}$ direction, making the δNi_2Si lattice coincident with the Cu matrix lattice.

The lattice correspondence between the δ precipitate and the Cu matrix, with the OR of $(110)_{Cu} \| (100)_{\delta}$ and $[001]_{Cu} \| [001]_{\delta}$, is schematically illustrated in Fig. 6a. Fig. 6b shows a continuum representation of the lattice strain of Fig. 6a. The circle (Cu plane) is transformed into an ellipse (δ plane) and a small rotation (θ) produces an invariant.

According to the geometrical relationship $(110)_{Cu}$ ||$(100)_{\delta}$ and $[001]_{Cu}$ ||$[001]_{\delta}$, the rotation angle, σ, to obtain $(\bar{1}11)_{Cu}/(021)_{\delta}$ can be calculated by:

$$\sigma = \mathrm{ArcTan}\left(\sqrt{2}/2\right) - \mathrm{ArcTan}(b_{\delta}/2c_{\delta}) \quad (2)$$

The difference between σ and θ signifies the angular deviation between the predicted OR and the actual OR_{RP}. Fig. 6c is a contour map showing the angular deviation (σ-θ) for different combinations of b_{δ} and c_{δ}. It is shown that the maximum possible angular deviation between the predicted OR and the measured OR_{RP} is quite small (≤ 0.3°) when the lattice changes from NP to RP. As the most probable path of the evolution of b_{δ} and c_{δ} during aging is the diagonally downwards from left to right, the angular deviation between the predicted OR and the measured OR_{RP} is less than 0.1°. In other words, the prediction of the 2DIL theory matches the experimental results very well.

It is interesting to point out that the above rotation transformation of the OR in the δ/Cu system is similar to the Bain-to-NW transformation in bcc/fcc systems (transformation from the Bain and Dunkirk [27] OR to the Nishiyama [28] – Wassermann [29] OR) [25]. Fig. 7a is a composite stereogram showing the four pairs of conjugate planes in bcc/fcc systems, with the Bain OR of $\{111\}_f/\{110\}_b$ (the subscripts *f* and *b* represent fcc and bcc, respectively) [27]. Rotating one pair of conjugate planes by 9.74° around $[110]_f$ or $[\bar{1}10]_f$ leads to the NW OR [28]. Similarly, the four pairs of conjugate planes in the δ/Cu system ($\{111\}_{Cu}/\{301\}_{\delta}$ and $\{111\}_{Cu}/\{021\}_{\delta}$) can also be displayed on a composite stereogram in the same reference frame ($[001]_{Cu}$ is equivalent to $[001]_f$), as shown in Fig.

7b. A rotation around $[110]_{Cu}$ or $[\bar{1}10]_{Cu}$ can make one pair of conjugate planes parallel, achieving a similar distribution as in Fig. 7a. The OR_{NP} in the δ/Cu system can be treated as a quasi-Bain OR, while the OR_{RP} as a quasi-NW OR. Fig. 7b shows that the angle differences between the conjugate planes in the δ/Cu system are about 3° smaller than that in the bcc/fcc system, indicating that a small rotation could result in a transformation from the quasi-Bain OR to the quasi-NW OR. In other words, the difference in thermodynamic energy between the quasi-Bain OR and the quasi-NW OR in the δ/Cu system is smaller than that between the Bain OR and the NW OR in the bcc/fcc system. This can explain the fact that the quasi-Bain OR between the NPs and the Cu matrix in the δ/Cu system has been observed, while the Bain OR has never been observed in conventional bcc/fcc systems.

The quasi-NW OR in the δ/Cu system can produce two OR variants, because both the clockwise and counterclockwise rotations can lead to a chiral symmetrical relationship. In other word, the transition from the OR_{NP} to the OR_{RP} can follow two paths. As shown in Fig. 7b, the two types of the quasi-NW OR are $\{111\}_{Cu}\|\{021\}_{\delta}$ and $\{111\}_{Cu}\|\{301\}_{\delta}$. Jia *et al*. [18] reported that there are six δ variants for each quasi-Bain OR. As a consequence, there would be 12 variants of plate-shaped δ lying on the $\{1\ 1\ 0\}_{Cu}$ planes in a crystalline Cu grain at the over-aging stage. Table 2 lists the 12 δ variants each calculated for the three different zone axes or beam directions.

3.4 Interpretation of morphology evolution by 3DIL theory

The 3DIL theory is a phenomenological theory of phase-transformation crystallography capable of explaining morphological features of precipitates when a measured OR is given [30-34]. It is more accurate than the 2DIL theory in mathematically describing the morphology of the precipitates during transformation. Fujii *et al.* [31] and Luo & Dahmen [32] successfully explained the morphologies of the Cr precipitates in Cu/Cr systems using the 3DIL theory. They obtained the invariant line and habit plane by solving the eigensystems of the transformation matrix. Specifically, the eigenvector with the least eigenstrain was regarded approximately as the invariant line. The habit plane was formed by the invariant line and another eigenvector with a small eigenstrain. The cross products of the eigenvectors were used to predict some of the major facets of the precipitates [30-32, 35].

We can apply the 3DIL theory to the Cu/δ system to explain the morphological features of the precipitates. Although the Cu/δ system is not a typical fcc/bcc system, we can borrow the concepts from the fcc/bcc system, namely Bain correspondence, Bain distortion and R_σ rotation (R_σ is the rotation matrix) to determine the transformation matrix. The terms generalized Bain correspondence and generalized Bain distortion are used here to extend these concepts to non-fcc/bcc systems.

Fig. 8 is schematic illustrations of the precipitation crystallography in the Cu/δ system based on the 3DIL model, using the OR of $(\bar{1}11)_{Cu}\|(021)_{\delta}$ and $[110]_{Cu}\|[100]_{\delta}$ as an example. The phase transformation with the OR_{NP} can be mathematically decomposed

into generalized Bain correspondence (*B*) (Fig. 8a), generalized Bain distortion (*D*) (Fig. 8b) and R_σ rotation (Fig. 8c).

The generalized Bain distortion matrix in the Cu matrix reference frame can be expressed as:

$$D_{Cu} = B^{-1} \cdot D_\delta \cdot B \tag{3}$$

where *B* is the generalized Bain matrix and D_δ is the generalized Bain distortion matrix in the δ reference frame, and their values are:

$$B = \begin{bmatrix} 1/3 & 1/3 & 0 \\ -1/2 & 1/2 & 0 \\ 0 & 0 & 1 \end{bmatrix} \tag{4}$$

and

$$D_\delta = \begin{bmatrix} \frac{a_\delta}{1.5\sqrt{2}a_{Cu}} & 0 & 0 \\ 0 & \frac{b_\delta}{\sqrt{2}a_{Cu}} & 0 \\ 0 & 0 & \frac{c_\delta}{a_{Cu}} \end{bmatrix} \tag{5}$$

According to the geometrical relationship shown in Fig. 8b and given the lattice parameters of a_{Cu}=3.615 Å, a_δ=7.06Å, b_δ=4.99Å and c_δ=3.72Å, the rotation matrix can be expressed as:

$$R_\sigma = \begin{bmatrix} 0.99985 & 0.00015 & 0.01746 \\ 0.00015 & 0.99985 & -0.01746 \\ -0.01746 & 0.01746 & 0.99970 \end{bmatrix} \tag{6}$$

Given the relationship and values in Eq. (3)-(6), the phase transformation matrix can be obtained as:

$$A = R_\sigma \cdot D_{Cu} = \begin{bmatrix} 0.94820 & -0.02756 & 0.01796 \\ -0.02756 & 0.94820 & -0.01796 \\ -0.01704 & 0.01704 & 1.02873 \end{bmatrix} \tag{7}$$

Table 3 lists the calculated eigensystems (eigenvectors, eigenvalues, eignestrains and eigen planes) of the phase transformation matrix for the OR of $(\bar{1}11)_{Cu}||(021)_{\delta}$ and $[110]_{Cu}||[100]_{\delta}$, corresponding to the RPs shown in Fig. 9. For both the RPs in Figs. 9a and 9b and the RP in Fig. 9c (they have slightly different input lattice parameters), the strains along the eigenvectors *X1* and *X2* are small and so does the angle between them. *X3* is perpendicular to *X1* and *X2* and has a large strain. From the least-strain point of view, the plane containing *X1* and *X2*, the $(110)_{Cu}$ plane, can easily develop into the habit facet F1, with the *X3* being the thickness direction. Indeed, Fig. 9 shows that F1 is the habit plane, F2 is the major facet on the edge of the habit plane, and F4 is close to the measured plane $(\bar{1}\ 1\ 1.84)_{Cu}$, with a small difference of 3.69°. These eigenplanes can also be observed in Fig. 3.

Table 3 also lists the calculated eigensystems of the phase transformation matrix for the OR of $(111)_{Cu}||(301)_{\delta}$ and $[\bar{1}10]_{Cu}||[010]_{\delta}$, corresponding to the precipitates reported in the previous works [5, 22-24]. The phase transformation matrix for the OR was also determined using Eqs. (3)-(7) using values specific to the OR. The results show that the strains for the eigenvectors *X1'*, *X2'*, *X3'* are -0.6%, -4.7% and -2.4%, respectively, for the OR of $(111)_{Cu}||(301)_{\delta}$ and $[\bar{1}10]_{Cu}||[010]_{\delta}$. Only *X1'* has a small strain, while *X2'* and *X3'* have relatively large strains. This means that it is much easier for the precipitate to grow along *X1'* than along *X2'* and *X3'*. This prediction agrees well with the observations in the previous works [5, 22-24] that the discontinuous δ precipitates with the OR of

$(111)_{Cu}||(301)_{\delta}$ and $[\bar{1}10]_{Cu}||[010]_{\delta}$ lie on the $(111)_{Cu}$ planes and exhibit a fiber-like shape rather than a plate-like shape.

Actually, the lattice parameters of the precipitates change continuously during aging because of the diffusion nature of the phase transformation. Accordingly, the eigenvector with the smallest strain changes as well. Comparing with Fig.9a and 9b, The precipitate's growth path can be inferred from the observations of precipitates of different sizes. When the precipitate is small (Fig. 9a), the precipitate can grow much easily along the *X1* direction, because it has the smallest strain, leading to the formation of the F2 facet. When the precipitate becomes large (Fig. 9b), however, its lattice parameters become similar to those of the standard powder. The direction for the easiest growth changes to *X2*, and the F4 facet is formed.

For comparison, the OR predicted by the 2DIL theory was also used to calculate the eigenvectors *V1*, *V2* and *V3* and they are also listed in Table 3. Apparently, an eigenvector strictly satisfying the invariant line condition was obtained due to the self-consistency of the 2DIL model. However, the 2DIL model cannot used to examine the facets except for the habit plane. The 3DIL theory is needed to interpret the precipitate morphology.

4. Conclusions

1. The main precipitates of the Cu-3.0Ni-0.72Si alloy at the early stage of aging are fine metastable $(Cu,Ni)_2Si$ precipitates coherent with the matrix. The $(Cu,Ni)_2Si$

precipitates have a δNi_2Si structure, with a portion of the Ni atoms substituted by Cu atoms. During growth, the core region of the metastable $(Cu,Ni)_2Si$ precipitate transforms into stable δNi_2Si, while a layer of metastable $(Cu,Ni)_2Si$ still exists around the core.

2. The evolution of the ORs between the precipitates and the matrix in the Cu/δ system is similar to the Bain-to-NW transformation in conventional fcc/bcc systems. The OR between the metastable NP ($(Cu,Ni)_2Si$) and the Cu matrix is a quasi-Bain OR, $(110)_{Cu}||(100)_\delta$ and $[001]_{Cu}||[001]_\delta$, with four pairs of parallel conjugate planes, $(\bar{3}\,01)_\delta||(\bar{1}\bar{1}1)_{Cu}$, $(301)_\delta||(111)_{Cu}$, $(021)_\delta||(\bar{1}11)_{Cu}$, and $(0\bar{2}1)_\delta||(1\bar{1}1)_{Cu}$. With the growth of the metastable NP to the stable RP (δNi_2Si), the quasi-Bain OR turns into a quasi-NW OR, $(\bar{1}\ 1\ 1)_{Cu}||(0\ 2\ 1)_\delta$ and $[1\ 1\ 0]_{Cu}||[1\ 0\ 0]_\delta$, with $(\bar{1}\ 1\ 1)_{Cu}\ \Gamma(\bar{3}\ 0\ 1)_\delta$, $(1\ 1\ 1)_{Cu}\Gamma(3\ 0\ 1)_\delta$, $(1\ \bar{1}\ 1)_{Cu}\Gamma(0\ \bar{2}\ 1)_\delta$. Twelve chiral δNi_2Si variants formed under this new quasi-NW OR. The conventional OR of $[\bar{1}10]_{Cu}||[010]_\delta$ and $(111)_{Cu}||(301)_\delta$ is another variant of the quasi-NW OR.

3. The RPs have a plate-like morphology. The broad facets are the habit plane $(1\ 0\ 0)_\delta$ and there are two pairs of flat facets, $(0\ 2\ 1)_\delta$ and $(0\ \bar{2}\ 1)_\delta$, at the edges of the habit plane.

4. The transformation from OR_{NP} to OR_{RP} can be successfully explained by the 2DIL model. The relationship between the morphologies and the ORs in the Cu/δ system can be well interpreted by the 3DIL model. The precipitates with the OR of $[110]_{Cu}||[100]_\delta$ and $(\bar{1}11)_{Cu}||(021)_\delta$ tend to grow two-dimensionally to form a plate-like shape, while those with the OR of $(111)_{Cu}||(301)_\delta$ and $[\bar{1}10]_{Cu}||[010]_\delta$ tend to grow

one-dimensionally to form a fiber-like shape.

Acknowledgement

We acknowledge financial support by the National Key R&D Program of China (Project No. 2017YFB0306105 , No. 2016YFB0301300) and the National Natural Science Foundation of China (No. U1637210). We also acknowledge the use of microscopes at the Advanced Research Centre at Central South University.

References

[1] C. MG, Electrical conductor alloy Electr World 89(1) (1927) 137.

[2] D. Zhao, Q.M. Dong, P. Liu, B.X. Kang, J.L. Huang, Z.H. Jin, Aging behavior of Cu–Ni–Si alloy, Materials Science and Engineering: A 361(1–2) (2003) 93-99.

[3] Q. Lei, Z. Li, T. Xiao, Y. Pang, Z.Q. Xiang, W.T. Qiu, Z. Xiao, A new ultrahigh strength Cu–Ni–Si alloy, Intermetallics 42 (2013) 77-84.

[4] T. Hu, J.H. Chen, J.Z. Liu, Z.R. Liu, C.L. Wu, The crystallographic and morphological evolution of the strengthening precipitates in Cu–Ni–Si alloys, Acta Materialia 61(4) (2013) 1210-1219.

[5] S.Z. Han, S.H. Lim, S. Kim, J. Lee, M. Goto, H.G. Kim, B. Han, K.H. Kim, Increasing strength and conductivity of Cu alloy through abnormal plastic deformation of an intermetallic compound, 6 (2016) 30907.

[6] Q. Lei, Z. Xiao, W. Hu, B. Derby, Z. Li, Phase transformation behaviors and properties of a high strength Cu-Ni-Si alloy, Materials Science and Engineering: A 697 (2017) 37-47.

[7] D.M. Zhao, Q.M. Dong, P. Liu, B.X. Kang, J.L. Huang, Z.H. Jin, Structure and strength of the age hardened Cu–Ni–Si alloy, Materials Chemistry and Physics 79(1) (2003) 81-86.

[8] R. Monzen, C. Watanabe, Microstructure and mechanical properties of Cu–Ni–Si alloys, Materials Science and Engineering: A 483-484 (2008) 117-119.

[9] S. Suzuki, N. Shibutani, K. Mimura, M. Isshiki, Y. Waseda, Improvement in strength and electrical conductivity of Cu–Ni–Si alloys by aging and cold rolling, Journal of Alloys and Compounds 417(1) (2006) 116-120.

[10] S.Z. Han, J. Kang, S.-D. Kim, S.-Y. Choi, H.G. Kim, J. Lee, K. Kim, S.H. Lim, B. Han, Reliable and cost effective design of intermetallic Ni2Si nanowires and direct characterization of its mechanical properties, Scientific Reports 5 (2015) 15050.

[11] R.W. D, G.E. G, N.V. F, The structure and associated properties of an age hardening copper alloy, Transactions of the Metallurgical Society of AIME 221(3) (1961) 503-512.

[12] O. M, The Investigation of the Equilibrium State of the Whole System Copper-Nickel-Silicon.The II. Report, J. Jpn. Inst. Met 3 (1939) 336-348.

[13] S. Lee, H. Matsunaga, X. Sauvage, Z. Horita, Strengthening of Cu–Ni–Si alloy using high-pressure torsion and aging, Materials Characterization 90 (2014) 62-70.

[14] C.M. G, Copper Hardened by New Method, BRASS WORLD AND PLATERS' GUIDE 23(3) (1927) 77-79595.

[15] K. Toman, The structure of Ni2Si, Acta Crystallographica 5(3) (1952) 329-331.

[16] M.D. Teplitskiy, A.K. Nikolayev, N.I. Revina, Investigating of the dispersed particles in aging alloys of copper-nickel-silicon and copper-cobalt-silicon, Physics of Metals and Metallography 6(40) (1975) 99-103.

[17] T.-J. Cho, Y.-G. Kim, D.W. Endicott, A computer aided diffraction analysis in a Cu-base precipitation hardened alloy, Scripta Metallurgica et Materialia 30(3) (1994) 291-295.

[18] Y.-l. Jia, M.-p. Wang, C. Chen, Q.-y. Dong, S. Wang, Z. Li, Orientation and diffraction patterns of δ-Ni2Si precipitates in Cu–Ni–Si alloy, Journal of Alloys and Compounds 557(0) (2013) 147-151.

[19] S.A. Lockyer, F.W. Noble, Precipitate structure in a Cu-Ni-Si alloy, Journal of Materials Science 29(1) (1994) 218-226.

[20] S.A. Lockyer, F.W. Noble, Fatigue of precipitate strengthened Cu-Ni-Si alloy Materials Science and Technology 15(10) (1999) 1147-1153.

[21] Q. Lei, Z. Li, M.P. Wang, L. Zhang, Z. Xiao, Y.L. Jia, The evolution of microstructure in Cu–8.0Ni–1.8Si–0.15Mg alloy during aging, Materials Science and Engineering: A 527(24) (2010) 6728-6733.

[22] Q. Lei, Z. Li, A. Zhu, W. Qiu, S. Liang, The transformation behavior of Cu–8.0Ni–1.8Si–0.6Sn–0.15Mg alloy during isothermal heat treatment, Materials Characterization 62(9) (2011) 904-911.

[23] S. Semboshi, S. Sato, A. Iwase, T. Takasugi, Discontinuous precipitates in age-hardening Cu-Ni-Si alloys, Materials Characterization.

[24] S.Z. Han, J. Lee, M. Goto, S.H. Lim, J.H. Ahn, S. Kim, K. Kim, Increasing toughness by promoting discontinuous precipitation in Cu–Ni–Si alloys, Philosophical Magazine Letters 96(5) (2016) 196-203.

[25] U. Dahmen, Orientation relationships in precipitation systems, Acta Metallurgica 30(1) (1982) 63-73.

[26] U. Dahmen, P. Ferguson, K. Westmacott, Invariant line strain and needle-precipitate growth directions in Fe-Cu, Acta Metallurgica 32(5) (1984) 803-810.

[27] E.C. Bain, N. Dunkirk, The nature of martensite, trans. AIME 70(1) (1924) 25-47.

[28] Z. Nishiyama, X-ray investigation of the mechanism of the transformation from face centered cubic lattice to body centered cubic, Sci. Rep. Tohoku Univ. 23 (1934) 637.

[29] G. Wassermann, Influence of the--transformation of an irreversible Ni steel onto crystal orientation and tensile strength, Arch. Eisenhüttenwes 126 (1933) 647.

[30] C.P. Luo, G.C. Weatherly, The invariant line and precipitation in a Ni-45 wt% Cr alloy, Acta Metallurgica 35(8) (1987) 1963-1972.

[31] T. Fujii, H. Nakazawa, M. Kato, U. Dahmen, Crystallography and morphology of nanosized Cr particles in a Cu–0.2% Cr alloy, Acta Materialia 48(5) (2000) 1033-1045.

[32] C. Luo, U. Dahmen, Interface structure of faceted lath-shaped Cr precipitates in a Cu–0.33 wt% Cr alloy, Acta materialia 46(6) (1998) 2063-2081.

[33] D. Qiu, W.-Z. Zhang, A systematic study of irrational precipitation crystallography in fcc–bcc systems with an analytical O-line method, Philosophical Magazine 83(27) (2003) 3093-3116.

[34] C.P. Luo, U. Dahmen, K.H. Westmacott, Morphology and crystallography of Cr precipitates in a Cu-0.33 wt% Cr alloy, Acta Metallurgica et Materialia 42(6) (1994) 1923-1932.

[35] T. Fujii, T. Mori, M. Kato, Crystallography and morphology of needle-like α-Fe precipitate particles in a Cu matrix, Acta Metallurgica et Materialia 40(12) (1992) 3413-3420.

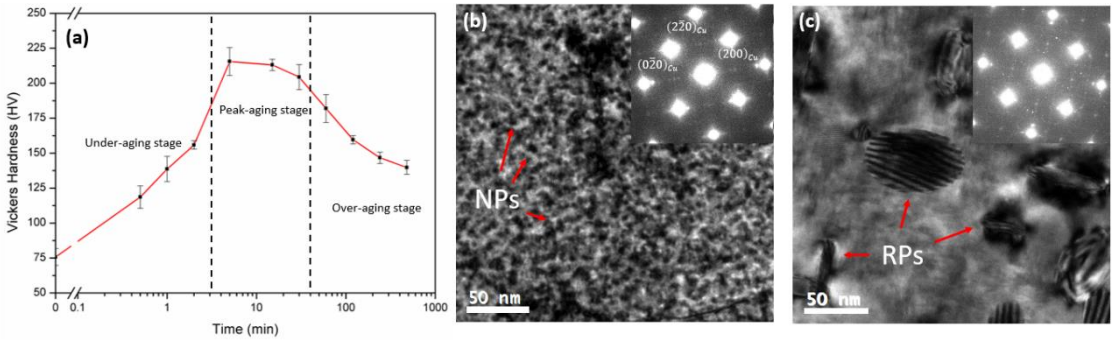

Fig.1 **(a)** Variation of hardness with aging time for the Cu-3.0Ni-0.72Si alloy aged at 600℃. Bright-field TEM images of the alloy aged for **(b)** 30 s and **(c)** 8 h, viewed along $[0\ 0\ 1]_{Cu}$.

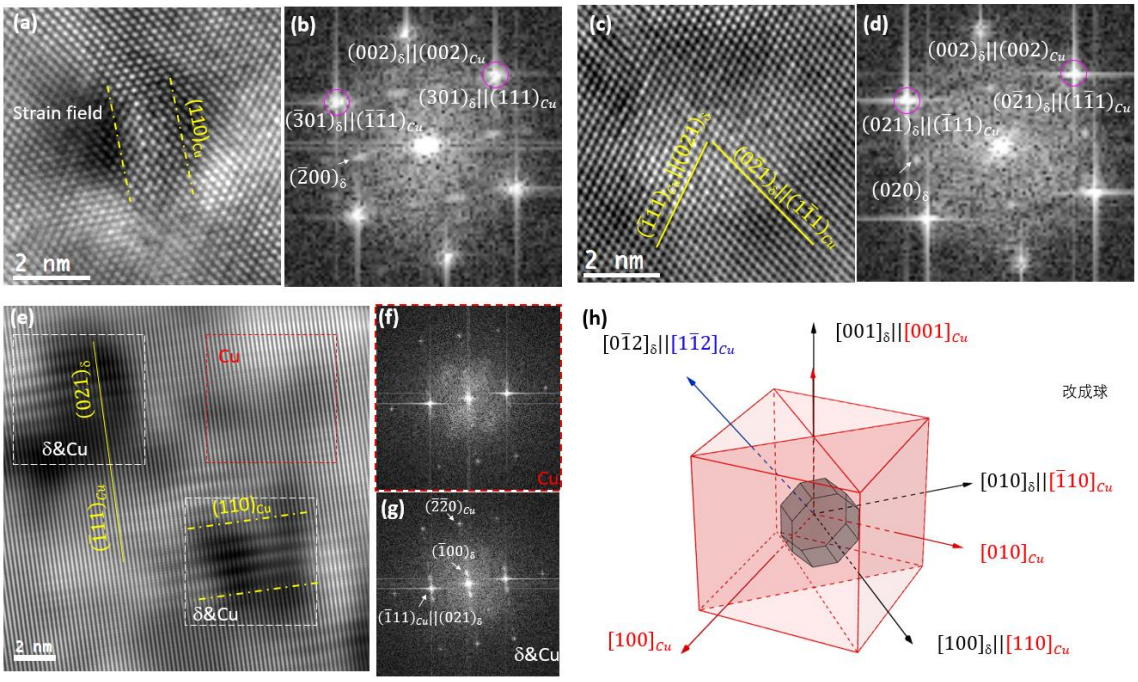

Fig. 2 HRTEM images and their corresponding FFT patterns of the Cu-3.0Ni-0.72Si alloy aged at 600℃ for 30 s: **(a)** HRTEM image taken from <1 1 0>$_{Cu}$, showing a single NP with edge-on habit planes (1 0 0)$_{\delta}$||(1 1 0)$_{Cu}$ (yellow dashed lines); **(b)** FFT pattern of (a), revealing the beam direction being [$\bar{1}$ 1 0]$_{Cu}$||[0 1 0]$_{\delta}$; **(c)** HRTEM image taken from <1 1 0>$_{Cu}$, showing a single NP with the habit plane perpendicular to the beam direction; **(d)** FFT pattern of (c), revealing the beam direction being [1 1 0]$_{Cu}$||[1 0 0]$_{\delta}$; **(e)** HRTEM image taken from <1 1 2>$_{Cu}$, showing two NPs with habit edge-on planes (1 0 0)$_{\delta}$||(1 1 0)$_{Cu}$ (yellow dashed lines); **(f)** FFT pattern of the red dash-line framed region in (e); **(g)** FFT pattern of the white dash-line framed region in (e), revealing the beam direction being [1 $\bar{1}$ 2]$_{Cu}$||[0 $\bar{1}$ 2]$_{\delta}$. **(h)** Schematic three-dimensional illustration of a NP showing its shape and OR$_{NP}$.

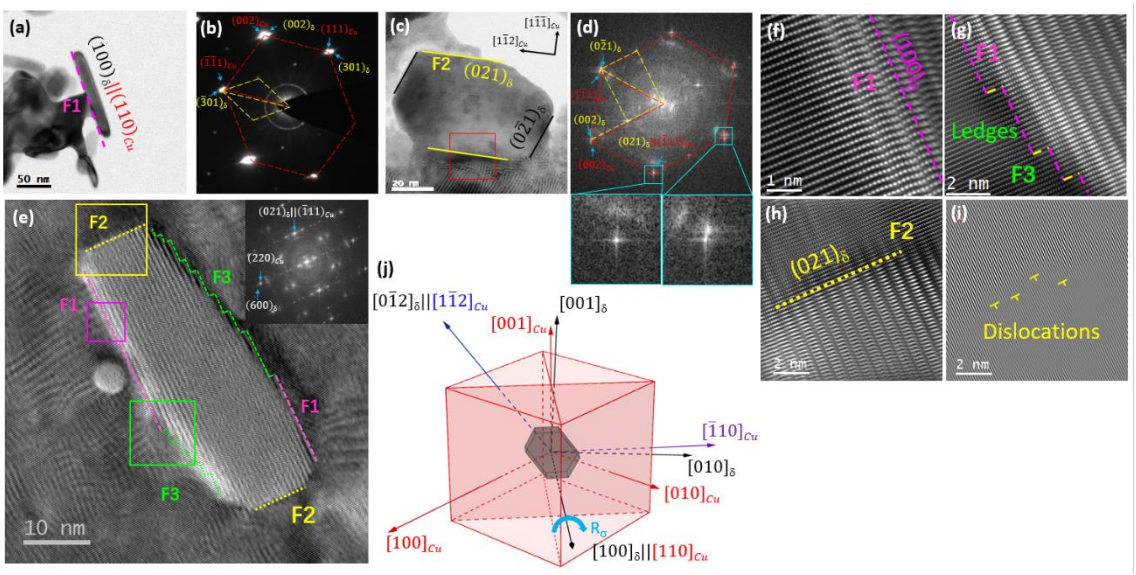

Fig. 3 HRTEM images and their corresponding FFT patterns of the Cu-3.0Ni-0.72Si alloy aged at 600℃ for 8 h: **(a)** Bright-field TEM image taken from <1 1 0>$_{Cu}$ showing a single RP with edge-on habit planes (1 0 0)$_{\delta}$||(1 1 0)$_{Cu}$ (pink dashed lines); **(b)** Selected-area electron diffraction patterns of (a) revealing the beam direction being $[\bar{1}\ 1\ 0]_{Cu}$||$[0\ 1\ 0]_{\delta}$; **(c)** Bright-field TEM image taken from <1 1 0>$_{Cu}$ showing a single RP with a habit plane perpendicular to the beam direction; **(d)** FFT pattern of the red line framed region in (c) revealing the beam direction being $[1\ 1\ 0]_{Cu}$||$[1\ 0\ 0]_{\delta}$; **(e)** HRTEM image taken from <1 1 2>$_{Cu}$ showing a RP with edge-on habit planes (1 0 0)$_{\delta}$||(1 1 0)$_{Cu}$ (pink dashed lines), with the inset FFT pattern revealing the beam direction being $[1\ \bar{1}\ 2]_{Cu}$||$[0\ \bar{1}\ 2]_{\delta}$; HRTEM images of **(f)** pink, **(g)** green and **(h)** luminous yellow framed areas in (e); **(i)** Inversed FFT images of (h) masking (2 2 0)$_{Cu}$ and (6 0 0)$_{\delta}$ spots. **(j)** Schematic three-dimensional illustration of a RP showing its shape and OR$_{RP}$.

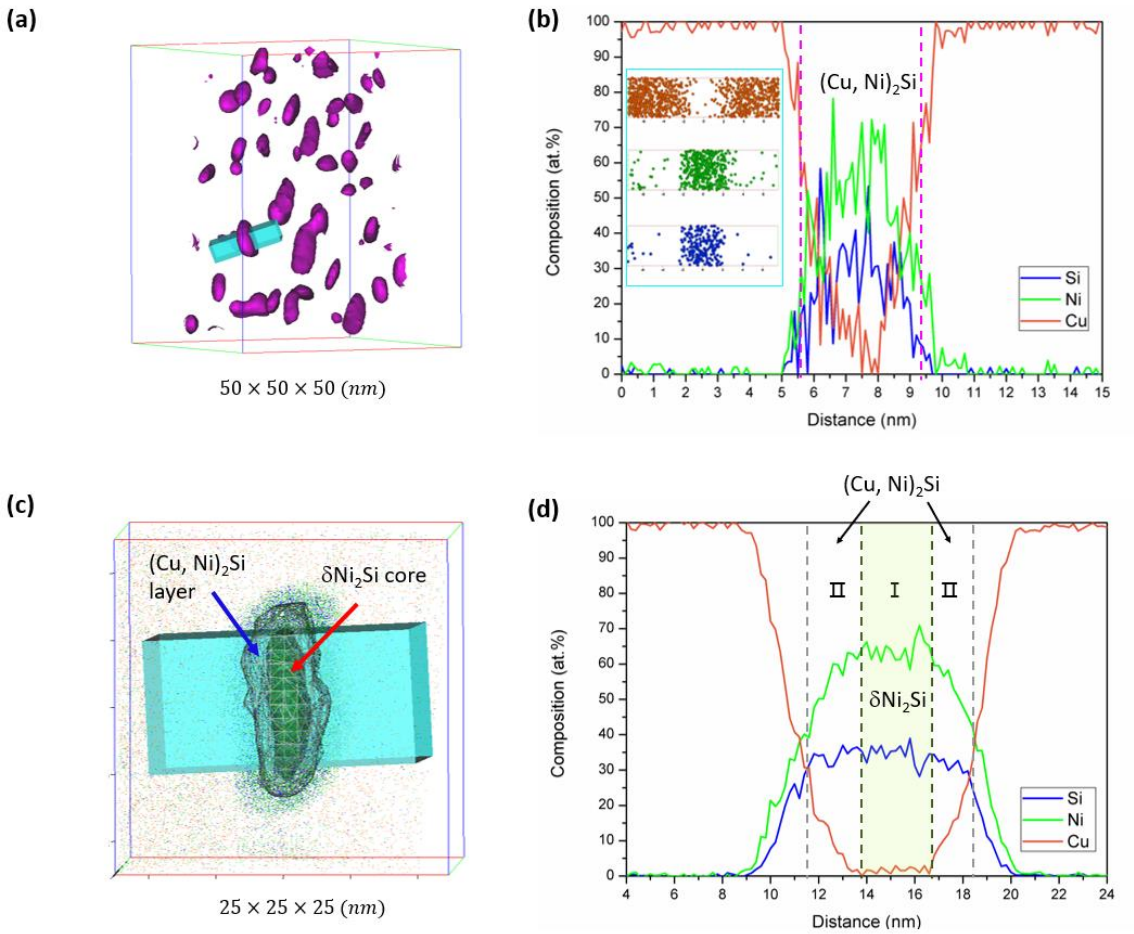

Fig. 4 Atom probe analysis showing the tomography and composition of the NP ((a) and (b)) and RP ((c) and (d)). The vertical dashed lines show the positions of the isoconcentration surfaces.

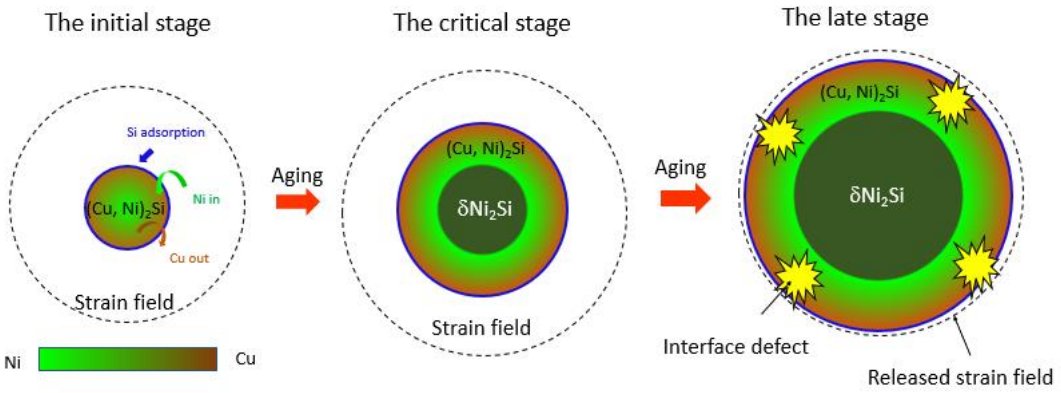

Fig. 5 Schematic diagram showing the coarsening of precipitates in Cu-Ni-Si alloys.

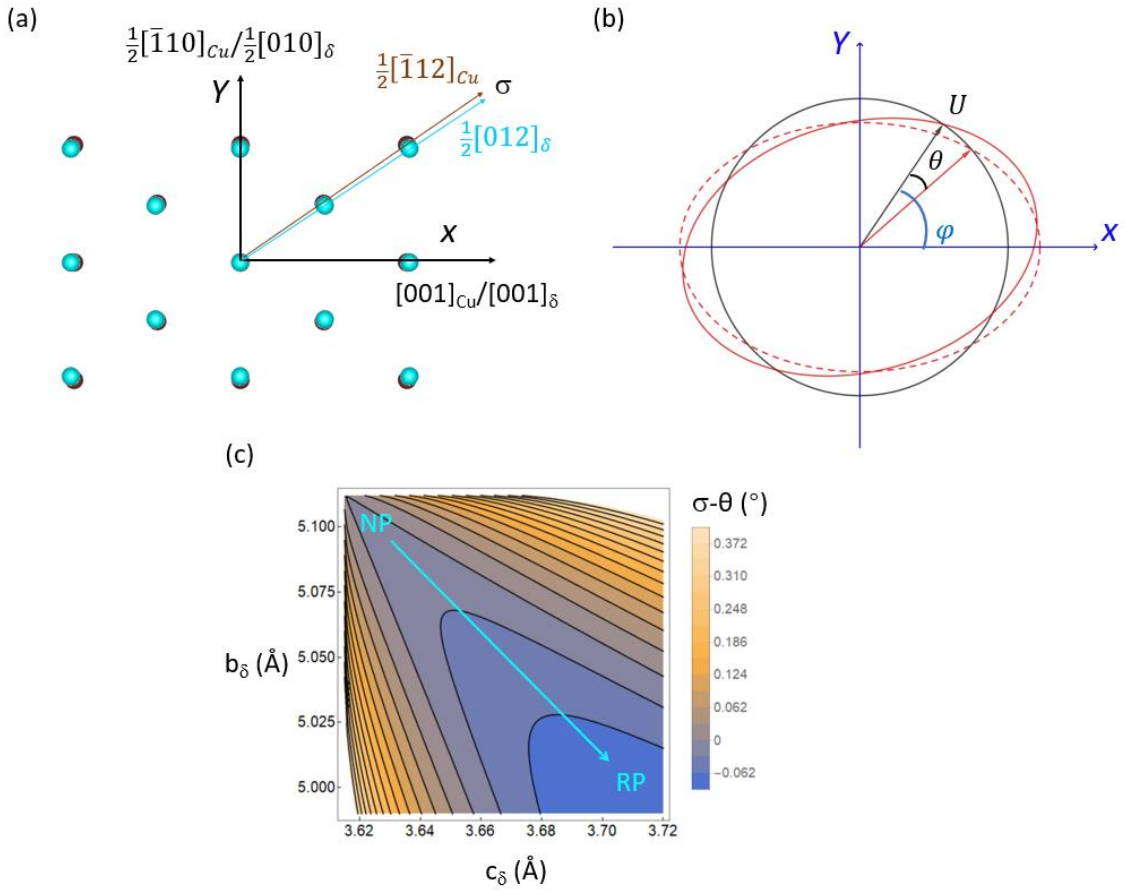

Fig. 6 **(a)** Schematic illustration of the lattice correspondence between the δ precipitate and the Cu matrix with OR $(1\ 1\ 0)_{Cu}\ ||(1\ 0\ 0)_{\delta}$ and $[0\ 0\ 1]_{Cu}\ ||[0\ 0\ 1]_{\delta}$. Cerulean: average positions of Ni/Si atoms. Earthy yellow: positions of Cu atoms. **(b)** Continuum representation of the lattice strain of (a). The circle (Cu plane) is transformed into an ellipse (δ plane) and a small rotation of θ produces an invariant U. **(c)** Contour map showing angular difference $(\sigma - \theta)$ against different lattice parameters of δNi_2Si.

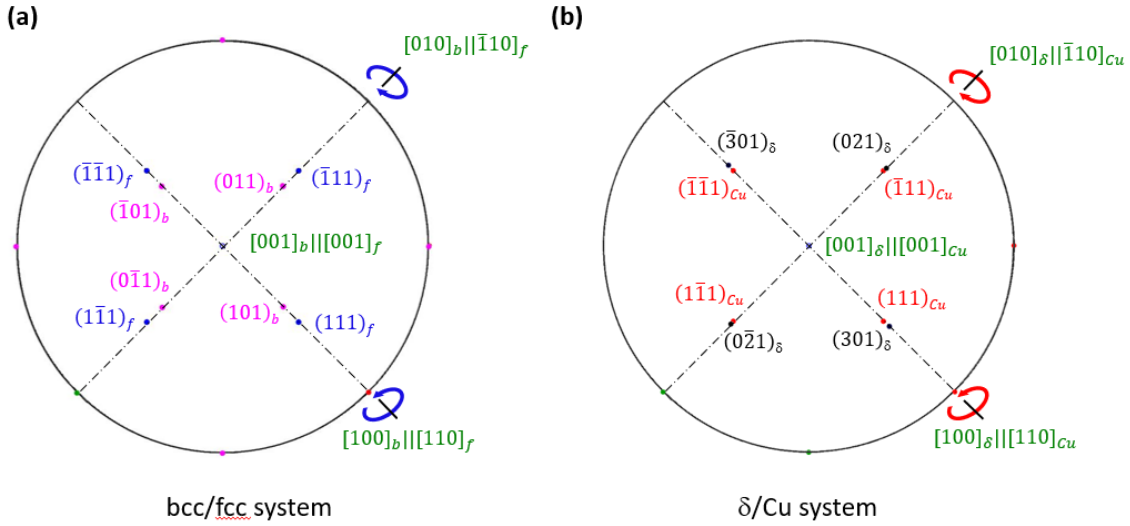

Fig. 7 Composite stereograms of **(a)** Bain OR in bcc/fcc systems and **(b)** quasi-Bain OR in the δ/Cu systems, showing that rotations around the axes lead to NW OR and quasi-NW OR, respectively.

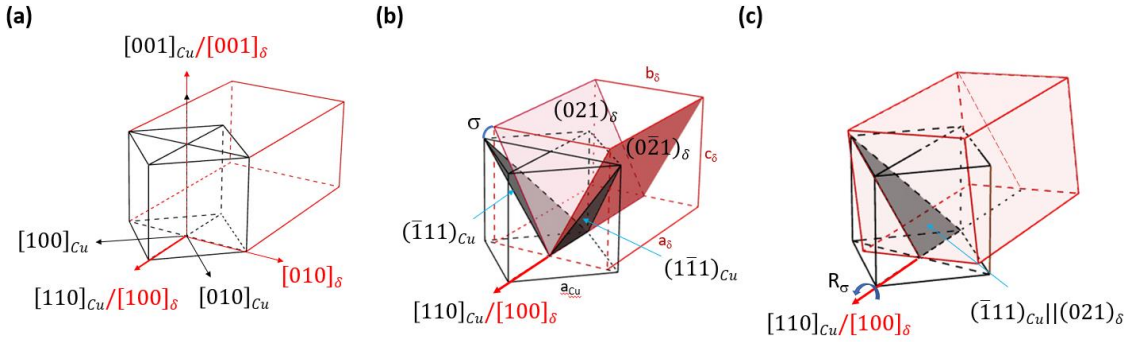

Fig.8 Schematic illustrations of the 3DIL precipitation crystallography model in the Cu/δ system: **(a)** generalized Bain correspondence, **(b)** generalized Bain distortion and **(c)** R_σ rotation resulting in the OR_{RP}.

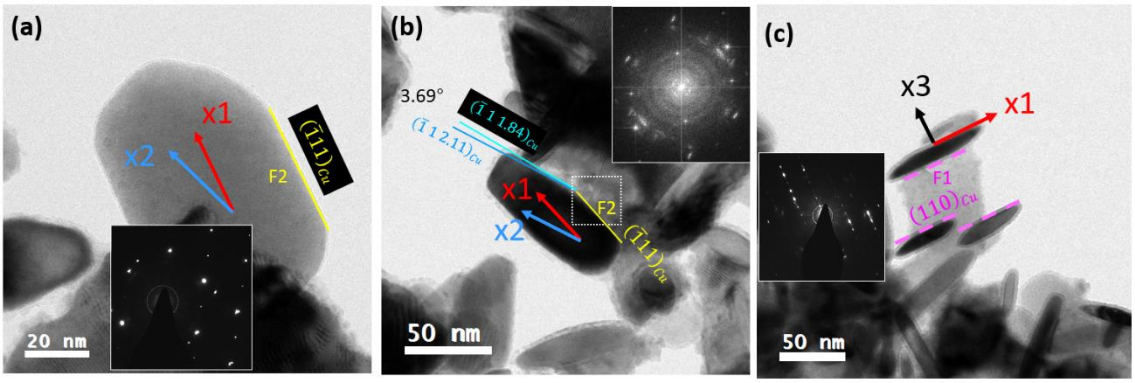

Fig.9 Bright-field TEM images showing RPs in the Cu-3.0Ni-0.72Si alloy, viewed along **(a)** <1 1 0>$_{Cu}$, **(b)** <1 1 0>$_{Cu}$ and **(c)** <1 1 1>$_{Cu}$.

Table 1 Lengths of the principal axes in the Cu/δ system at different aging stages (unit Å)*.

Corresponding principal directions	Matrix Cu	NPs	RPs	Toman's data
$[100]_\delta/\left[\frac{3}{2}\frac{3}{2}0\right]_{Cu}$	7.668	7.09~7.36	7.01~7.08	7.06
$[010]_\delta/[\bar{1}10]_{Cu}$	5.112	5.01~5.10	4.93~5.02	4.99
$[001]_\delta/[001]_{Cu}$	3.615	3.64~3.67	3.64~3.72	3.72

* The lattice parameter of the Cu matrix is 3.615Å. The length of the principal axis of δ was obtained from the HRTEM images, using a_{Cu}=3.615Å as the internal standard.

Table 2 Calculated zone axes of the 12 variants of precipitates for beam directions of $[110]_{Cu}$, $[111]_{Cu}$ and $[112]_{Cu}$ **

	Variant	$[110]_{Cu}$	$[111]_{Cu}$	$[112]_{Cu}$
P1	$[110]_{Cu}\|\|[100]_{\delta},(\bar{1}11)_{Cu}\|\|(021)_{\delta}$	$[100]_{\delta}$*	$[0.724\ 0.018\ 0.971]_{\delta}$	$[0.724\ 0.036\ 1.943]_{\delta}$
p2	$[110]_{Cu}\|\|[100]_{\delta},(1\bar{1}1)_{Cu}\|\|(0\bar{2}1)_{\delta}$	$[100]_{\delta}$*	$[0.724\ \overline{0.018}\ 0.971]_{\delta}$	$[0.724\ \overline{0.036}\ 1.943]_{\delta}$
p3	$[101]_{Cu}\|\|[100]_{\delta},(11\bar{1})_{Cu}\|\|(021)_{\delta}$	$[0.362\ \overline{0.530}\ \overline{0.954}]_{\delta}$	$[0.724\ \overline{0.018}\ \overline{0.971}]_{\delta}$	$[1.086\ 0.494\ \overline{0.988}]_{\delta}$
p4	$[101]_{Cu}\|\|[100]_{\delta},(\bar{1}11)_{Cu}\|\|(0\bar{2}1)_{\delta}$	$[0.362\ \overline{0.494}\ \overline{0.988}]_{\delta}$	$[0.724\ 0.018\ \overline{0.971}]_{\delta}$	$[1.086\ 0.530\ \overline{0.954}]_{\delta}$
p5	$[011]_{Cu}\|\|[100]_{\delta},(1\bar{1}1)_{Cu}\|\|(021)_{\delta}$	$[0.362\ \overline{0.494}\ 0.988]_{\delta}$	$[0.724\ 0.018\ 0.971]_{\delta}$	$[1.086\ 0.530\ 0.954]_{\delta}$
p6	$[011]_{Cu}\|\|[100]_{\delta},(11\bar{1})_{Cu}\|\|(0\bar{2}1)_{\delta}$	$[0.362\ \overline{0.530}\ 0.954]_{\delta}$	$[0.724\ \overline{0.018}\ 0.971]_{\delta}$	$[1.086\ 0.494\ 0.988]_{\delta}$
p7	$[\bar{1}10]_{Cu}\|\|[100]_{\delta};(11\bar{1})_{Cu}\|\|(021)_{\delta}$	$[0\ \overline{1.024}\ 0.034]_{\delta}$**	$[0\ \overline{1.006}\ 1.005]_{\delta}$	$[0\bar{1}2]_{\delta}$
p8	$[\bar{1}10_{Cu}\|\|[100]_{\delta},(111)_{Cu}\|\|(0\bar{2}1)_{\delta}$	$[0\ \overline{1.024}\ \overline{0.034}]_{\delta}$**	$[0\ \overline{1.042}\ 0.938]_{\delta}$	$[0\ \overline{1.060}\ 1.909]_{\delta}$
p9	$[10\bar{1}_{Cu}\|\|[100]_{\delta},(1\bar{1}1)_{Cu}\|\|(021)_{\delta}$	$[0.362\ \overline{0.494}\ 0.988]_{\delta}$	$[0\ \overline{1.006}\ 1.005]_{\delta}$	$[\overline{0.362}\ \overline{1.518}\ 1.022]_{\delta}$
p10	$[10\bar{1}_{Cu}\|\|[100]_{\delta},(111)_{Cu}\|\|(0\bar{2}1)_{\delta}$	$[0.362\ \overline{0.530}\ 0.954]_{\delta}$	$[0\ \overline{1.042}\ 0.938]_{\delta}$	$[\overline{0.362}\ \overline{1.554}\ 0.920]_{\delta}$
p11	$[01\bar{1}]_{Cu}\|\|[100]_{\delta},(111)_{Cu}\|\|(021)_{\delta}$	$[0.362\ \overline{0.530}\ \overline{0.954}]_{\delta}$	$[0\ \overline{1.042}\ \overline{0.938}]_{\delta}$	$[\overline{0.362}\ \overline{1.554}\ \overline{0.920}]_{\delta}$
p12	$[01\bar{1}]_{Cu}\|\|[100]_{\delta},(\bar{1}11)_{Cu}\|\|(0\bar{2}1)_{\delta}$	$[0.362\ \overline{0.494}\ \overline{0.988}]_{\delta}$	$[0\ \overline{1.006}\ \overline{1.005}]_{\delta}$	$[\overline{0.362}\ \overline{1.518}\ \overline{1.022}]_{\delta}$

** Lattice parameters used for calculations: a_{Cu}=3.615Å, a_{δ}=7.06Å, b_{δ}=4.99Å, c_{δ}=3.72Å.

Table 3 Eigenvectors, eigenvalues, eigenstrains and eigenplanes calculated by the 3DIL theory for several selected precipitates.

Precipitates	Lattice parameters	ORs	Eigenvectors	Eigenvalues	Eigenstrains	Eigenplanes
In Fig.9a	a_{δ}=7.06 b_{δ}=5.02 c_{δ}=3.67	$[110]_{Cu}\|\|[100]_{\delta}$ $(\bar{1}11)_{Cu}\|\|(021)_{\delta}$	**X1=$[1\bar{1}2]_{Cu}$** X2=$[1\ \bar{1}\ 0.96]_{Cu}$ X3=$[110]_{Cu}$	**1.004** 0.993 0.921	**0.4%** -0.7% -7.9%	$F1=X1\times X2=(110)_{Cu}$ $F2=X1\times X3=(\bar{1}11)_{Cu}$
In Fig.9b and c	a_{δ}=7.06 b_{δ}=4.99 c_{δ}=3.72	$[110]_{Cu}\|\|[100]_{\delta}$ $(\bar{1}11)_{Cu}\|\|(021)_{\delta}$	X1=$[1\bar{1}2]_{Cu}$ **X2=$[1\ \bar{1}\ 0.94]_{Cu}$** X3=$[110]_{Cu}$	1.012 **0.993** 0.921	1.2% **-0.7%** -7.9%	$F1=X1\times X2=(110)_{Cu}$ $F2=X1\times X3=(\bar{1}11)_{Cu}$ $F4=X2\times X3=$ $(\bar{1}\ 1\ 2.11)_{Cu}$~3.69° measured$(\bar{1}\ 1\ 1.84)_{Cu}$
In ref[5,22-24]	a_{δ}=7.06 b_{δ}=4.99 c_{δ}=3.72	$[\bar{1}10]_{Cu}\|\|[010]_{\delta}$ $(111)_{Cu}\|\|(301)$	X1′=$[\bar{1}\bar{1}2]_{Cu}$ X2′=$[11\overline{0.89}]_{Cu}$ X3′=$[\bar{1}10]_{Cu}$	0.994 0.953 0.976	-0.6% -4.7% -2.4%	$X1'\times X3'=(111)_{Cu}$ $X1'\times X2'=(\bar{1}10)_{Cu}$
Input predicted OR	a_{δ}=7.06 b_{δ}=4.99 c_{δ}=3.72	$[110]_{Cu}\|\|[100]_{\delta}$ $(111)_{Cu}\|\|(0\ 2\ 0.996$ with 0.095° away from $(021)_{\delta}$	V1=$[1\ \bar{1}\ 1.49]_{Cu}$ **V2=$[1\ \bar{1}\ 1.28]_{Cu}$** V3=$[110]_{Cu}$	1.004 **1.000** 0.9206	0.4% **0%** -7.94%	$V1\times V2=(110)_{Cu}$